The International Journal of Advanced Manufacturing Technology (2020) 107:145–156
https://doi.org/10.1007/s00170-020-05053-y

ORIGINAL ARTICLE

Experiment on carbon fiber–reinforced plastic cutting by abrasive waterjet with specific emphasis on surface morphology

Xin Li [1,2] · Xiaofeng Ruan [1,2] · Jialin Zou [1,2] · Xinping Long [1,2] · Zhengwen Chen [3]

Received: 4 September 2019 / Accepted: 30 January 2020 / Published online: 13 February 2020

Abstract
In the machining of carbon fiber–reinforced plastic by abrasive waterjet, the surface morphology of the cutting front directly reflects the processing quality. So in this study, the changes in the topography and surface roughness of the cutting front as a result of variations in five operational parameters, namely, the traverse speed, abrasive mass flow rate, waterjet pressure, standoff distance, and sample thickness, were experimentally studied with the aid of μscan laser confocal microscopy. It was found that periodic stripes and grooves appeared in the traverse direction from observations of three-dimensional surface morphology. And the analysis of the surface roughness revealed that there were three distinct cutting regions along the penetration direction, namely, an initial damage region at the jet entry, a smooth cutting region in the intervening cutting area, and a rough cutting region near the jet exit. According to the three distinct regions in the penetration direction, a three-zone cutting front model was proposed. A high-quality machined surface could be obtained by extending the smooth cutting zone through the appropriate choice of process parameters. Therefore, the influences of the above five parameters on the length of the smooth cutting zone were also investigated, and recommendations are proposed for process control.

Keywords Abrasive waterjet · Carbon fiber–reinforced plastic · Kerf profile · Surface roughness

1 Introduction

Carbon fiber–reinforced plastic (CFRP) is a composite material that has been increasingly used owing to its outstanding strength and inherent low density [1]. However, the discontinuous nature, non-uniformity, and anisotropy of CFRP make it a challenging task to process this material efficiently while maintaining high surface quality [2]. Furthermore, inappropriate cutting methods may even lead to the material damage and performance reduction such as delamination, internal cracking, and fiber pull-out. Traditional processing methods result in not only low cutting quality but also low efficiency [3], whereas some non-traditional methods, such as laser cutting technology, have been found to produce protruding fibers as a result of thermal distortion [4]. The unique "cold" abrasive waterjet (AWJ) technology was first proposed by the British Hydrodynamics Research Association in the mid-1980s. They proposed a method by which abrasive particles were accelerated by a stream of water, and the resulting coherent slurry jet of abrasive particles and water was used for materials processing. Mazurkiewicz [5] reported that this technology had greatly enhanced the cutting capability of the jet and made it possible to process hard and brittle materials at pressures of less than 70 MPa. In comparison with traditional and other non-traditional processing technologies, AWJ machining exhibits great advantages owing to its efficiency, versatility, and the high quality of the finished machined surface, especially as it avoids thermal deformation of the workpiece [6, 7]. Therefore, AWJ machining is an ideal processing method for composite materials, including CFRP.

In general, the process efficiency of AWJ machining and the resulting surface quality are affected by parameters such as the traverse speed, waterjet pressure, standoff distance,

✉ Xinping Long
xplong@whu.edu.cn

[1] Hubei Key Laboratory of Waterjet Theory and New Technology, Wuhan University, Wuhan 430072, China

[2] School of Power and Mechanical Engineering, Wuhan University, Hubei 430072, China

[3] Hefei General Machinery Research Institute, Hefei 230031, China

abrasive grit size, and abrasive flow rate [8]. In order to study the hole processing quality of CFRP sheets by AWJ, Kunlapat et al. [9] carried out an experiment and founded that the traverse speed had a profound effect on the kerf profile, whereas the waterjet pressure and abrasive mass flow rate had insignificant effects. High overall hole quality was achieved at a moderate traverse speed and a low waterjet pressure. Li et al. [10] conducted a study of radial-mode AWJ turning of short CFRP pieces to understand the relationship between machining performance and the cutting parameters; it was founded that the surface roughness (Ra) was related to the cutting depth and a higher rotational speed improved the surface quality. Alberdi et al. [11] also reported that the traverse speed was an important factor in roughness analysis by carried out an experiment. The experiment conducted by Liu et al. [12] indicted that the cutting depth was maximum with standoff distance of 5.5 mm, but the effect on the surface roughness was not obvious in the range of 1–10 mm. Therefore, the material quality of CFRP is sensitive to the machining parameters, and process control is of great significance.

In order to have a clear understanding of the influence of various parameters on the cutting process, several material-removal mechanisms and process models have been developed for process control and optimization [13–15]. Current research on models mainly focuses on ductile and brittle materials and is based on erosion theory [16], energy methods [17], and fracture mechanics [18]. Among these studies, two main models of the penetration direction have been proposed, namely, the two-stage impact zone model developed by Zeng and Kim [19] and the three-zone cutting front model proposed by Arola and Ramulu [20, 21], respectively. In the two-stage impact zone model, the cutting front was divided into direct and secondary impact zones according to the respective mechanisms of material removal. As for the three-zone cutting front model, three distinct regions were observed via visualization of the surface that was created, namely, an initial damage region (IDR) at the jet entry, an intermediate smooth cutting region (SCR), and a rough cutting region (RCR) adjacent to the jet exit. Although several studies on the processing of CFRP by AWJ have been conducted, these were often limited to a parametric analysis of kerf depth and taper. Furthermore, little research has been found that performed a detailed analysis of the process mechanism and cutting front morphology in AWJ machining of CFRP. This has to some extent hindered the processing of CFRP by AWJ technology. Hence, in this study, an examination of kerf profiles in AWJ cutting of CFRP was conducted by μscan laser confocal microscopy, and the effects of process parameters on surface roughness were studied. In addition, a model of the machining of CFRP is proposed, which was inspired by Arola and Ramulu's [20] three-zone cutting front model, from which recommendations are made on selecting the optimum cutting parameters for practical applications.

2 Experimentation and procedure

2.1 Material

In this study, CFRP containing 12 layers of carbon fiber with the T300 composition was used as the target material. The layered structure of the carbon fiber composite material, as well as the anisotropy between the layers, has made it difficult to process this material with high efficiency and high quality by traditional processing methods. The workpieces used in this study had thicknesses of 2.2 mm, 4.5 mm, 6.8 mm, 8.8 mm, and 11.0 mm, respectively. All machining was conducted with garnet abrasives with a mesh size of #80, which have the great advantages of moderate hardness, stable physical and chemical properties, etc.

2.2 Experimental equipment

The experiments were conducted on a cantilever CNC AWJ machine equipped with a WJQG37 cutting platform, a DPSB9-3040 intensifier pump, a CNC system, and an abrasive feeding system. The intensifier pump was used to pressurize filtered and softened water with a maximum pressure of 500 MPa. Then, the water was piped to a water cutting head of the cutting platform and exited through a sapphire orifice. At the same time, the abrasive and air from the abrasive feeding system were also delivered to the water cutting head and were entrained by the high-velocity water flow. Conceptually, this technique operates like a jet pump, and the pressurized abrasive water jet stream was used as an erosive medium to process the workpiece below. The cutting head and the workpiece were operated by the five-axis linkage water cutting machine to complete the preset process.

2.3 Cutting procedure

In these experiments, the process parameters in the AWJ machining procedure were selected on the basis of previous research into AWJ machining [16, 19]. As shown in Table 1, the parameters that were investigated included the traverse speed, abrasive mass flow rate, waterjet pressure, standoff distance, and sample thickness. It should be noted that the selection of the standoff distance was to keep the nozzle from rubbing the material considering the need to manufacture large specimens with complex shapes in industrial production, although a smaller standoff distance was found to be preferred [20]. And Yanaida [22] has reported that the length of the initial region of the non-submerged jet of high-pressure water is about 65 to 135 times of the diameter of the nozzle, which is much higher than the range of standoff distance selected in this paper. By controlled variation of the parameters, a total of 366 tests were performed, and the corresponding processed workpieces were obtained.

Table 1 Machining parameters selected for abrasive waterjet (AWJ) cutting

AWJ cutting parameter	Data					
Traverse speed u (mm·min^{-1})	800	600	400	200	100	50
Abrasive mass flow rate m_a (g·min^{-1})	1239	987	663	354		
Waterjet pressure p (MPa)	450	420	380	350	320	300
Standoff distance L (mm)	5	10	15	20		
Sample thickness d (mm)	2.2	4.5	6.8	8.8	11.0	

Figure 1 shows a CFRP workpiece subjected to cutting with the cutting parameters displayed on its surface, where the x-axis represents the feed direction, the y-axis represents the jet penetration direction, and the z-axis represents the direction in which the height of the cutting front fluctuated.

2.4 Measurement of landscape profiles

The surface morphology of the cutting front was measured by μscan laser confocal microscopy with an accuracy of 10 nm. In comparison with the case in other cutting methods, the changes in the roughness of the AWJ cutting front in the traverse direction were not obvious owing to the high periodicity of the stripes [7, 23]. In order to identify a suitable length range for measurements in the feed direction, sections with lengths of 30 mm and 40 mm were selected to measure the respective surface morphologies, and the results were compared. It was found that the section with a length of 30 mm contained at least 20 cycles, which was a large enough number to meet the accuracy requirements of this measurement. Therefore, in order to reduce the measurement workload, a section of the cutting front with a length of 30 mm in the feed direction was selected to acquire the kerf profile of the CFRP workpiece, which is sketched in Fig. 2. A pronounced periodic stripe structure can be seen in the x-direction, whereas in the y-direction a stripe structure is more obvious in the lower part, which indicates that the surface roughness seems to have changed with the penetration depth. According to our previous study, the resolution of the laser confocal microscope has no significant effect on the measurement of roughness. Hence, in this study, a microscope resolution of 30 μm × 30 μm and a sampling frequency of 500 Hz were selected according to the recommended values for the scanning device and our previous study.

In order to quantify the quality of the surface morphology, the variable Ra was used to denote the surface roughness of the cutting front in this paper. Here, Ra [8, 24] is the arithmetic average value of the absolute distance between a point on the contour line and the baseline in the measurement direction (z-direction in Fig. 1) within the sampling length, as sketched in Fig. 3 and mathematically defined by Eq. (1):

$$Ra = \frac{1}{n}\sum_{i=1}^{n}|h_i| \tag{1}$$

where n is the sampling number and h_i is the absolute distance between the profile curve and the baseline.

In order to determine the value of Ra along the jet penetration direction, several parallel horizontal lines were selected on the cutting front used for measurement, as shown in Fig. 4. The distances between the horizontal lines were 30 μm,

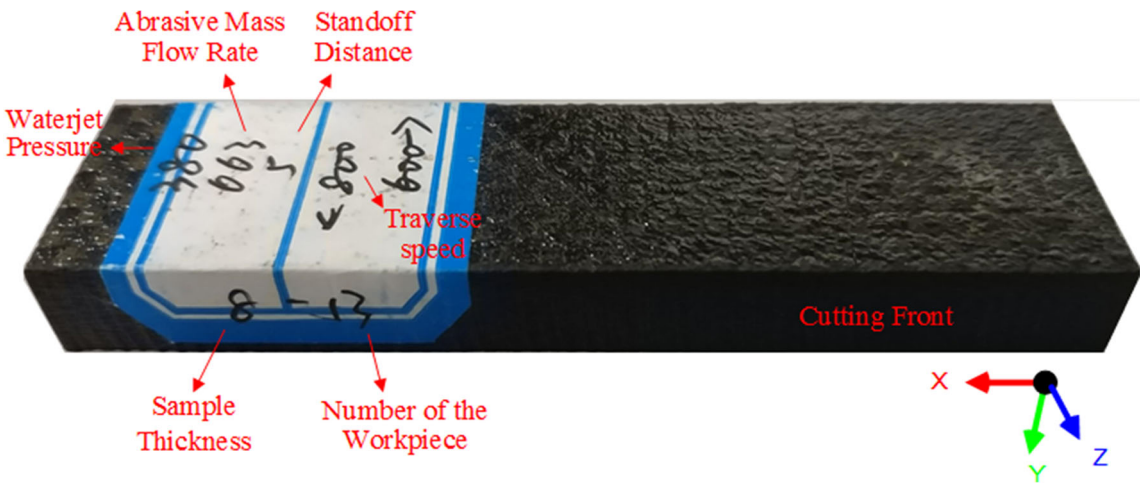

Fig. 1 Sample of carbon fiber–reinforced plastic (CFRP) workpiece subjected to AWJ cutting

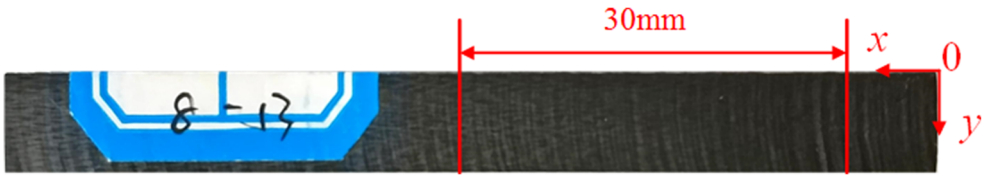

Fig. 2 Scanning range of the μscan laser confocal microscope

according to the resolution of the microscope. Thereby, the profile curves of the chosen parallel lines on the cutting front were acquired, of which one is shown in Fig. 5.

The greatest difficulty in the determination of Ra is the establishment of the baseline. In general, the contour signal can be decomposed into long-wave and short-wave components by a filtering operation, and the contour of the long-wave signal can be used as the baseline. In this study, a B-spline preprocessed Gaussian filter was chosen as the filtering operation to process the height fluctuation data and determine the surface roughness of the cutting front, which was achieved using the self-developed program PSAWJ based on Fortran 95/2003. The theory and algorithm of the B-spline analysis module in this program are based on *The NURBS Book* [25]. Gaussian filtering uses a standard filtering kernel function to filter surface roughness. By processing the measurement data, the Ra value of the CFRP cutting front was determined.

3 Results and discussion

The results for the morphology and surface roughness of the cutting front, which were used to facilitate the analysis of the influence of the process parameters on the quality of the machined surface, are shown and discussed below.

3.1 Observation of machined surface

As shown in Figs. 6, 7, 8, 9, and 10, the topography of the surface that was created was reconstructed from the height distribution data for the cutting front acquired by μscan laser confocal microscopy. The morphology of the cutting front can be observed visually in the 3D views, including the waviness patterns or stripes and grooves on the surface of the kerf. In addition, the stripes and grooves seemed to exhibit a certain periodicity in the feed direction, which indicated that the AWJ cutting process was cyclical, from the cyclical kerf profile. The topography of the CFRP sample seemed to be similar to that of traditional materials machined by AWJ, but different materials displayed cutting fronts with different characteristics in detail [16].

It can be seen from Figs. 6, 7, 8, 9, and 10 that different kerf profiles were obtained under different working conditions. Figure 6 illustrates that a fast traverse speed may result in more pronounced grooves in the feed direction and a rougher overall cutting front. The kerf profiles were different at different mass flow rates, as shown in Fig. 7, but the relationship is not obvious. As for the waterjet pressure, the effect is also not very apparent, as seen from Fig. 8. Figure 9 shows that surface grooves were more obvious at a small standoff distance, which was probably due to mechanical vibration of the jet perpendicular to the penetration direction. The kerf profiles for different sample thicknesses are shown in Fig. 10, and the waviness pattern became more obvious at a greater depth in the penetration direction as the sample thickness increased, which was probably because the jet energy was insufficient to destroy and remove the material efficiently as the penetration depth increased. According to these figures, the surface morphology changed with the operational parameters, including the fluctuations in height along the jet penetration direction and the periodicity of incisions in the feed direction. Therefore, the surface morphology of the cutting front was critically correlated with variations in the process parameters. However, the specific

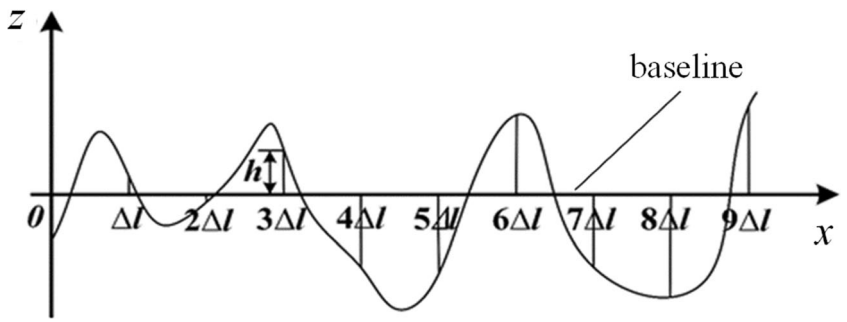

Fig. 3 Schematic diagram of surface roughness

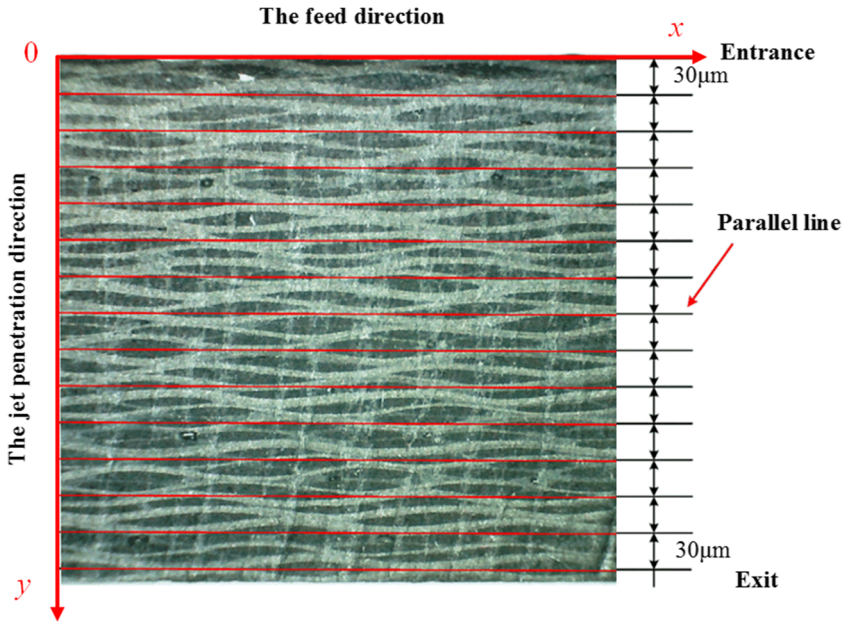

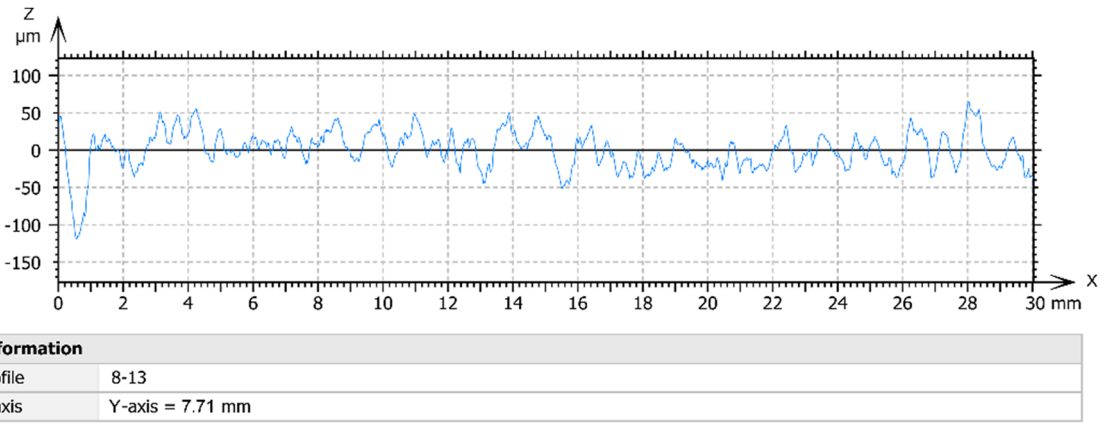

Information	
Profile	8-13
T-axis	Y-axis = 7.71 mm

Fig. 4 Parallel lines on the cutting front

Fig. 5 Profile curve of a selected parallel line on the cutting front

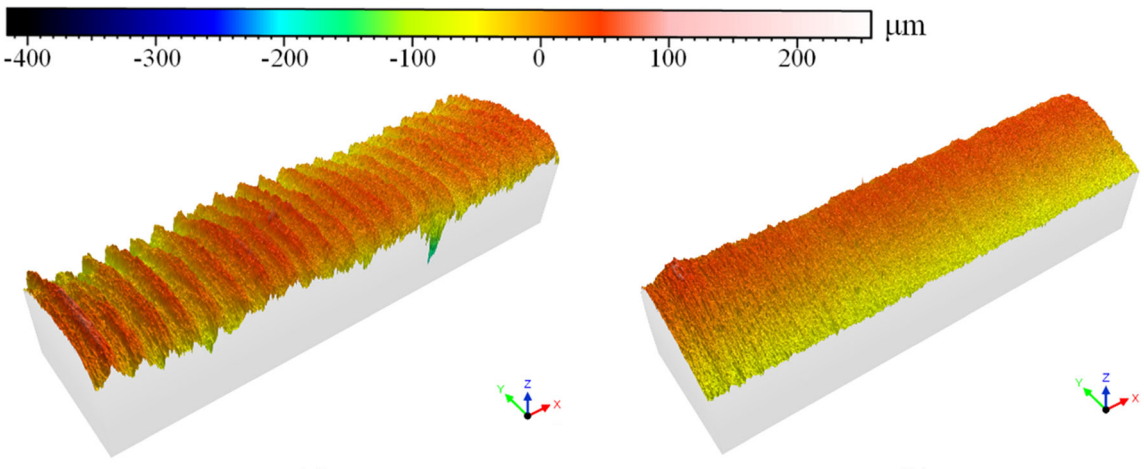

Fig. 6 3D views of the cutting front at different traverse speeds: **a** $u = 800$ mm/min; **b** $u = 50$ mm/min ($m_a = 663$ g/min, $p = 450$ MPa, $L = 5$ mm, $d = 8.8$ mm)

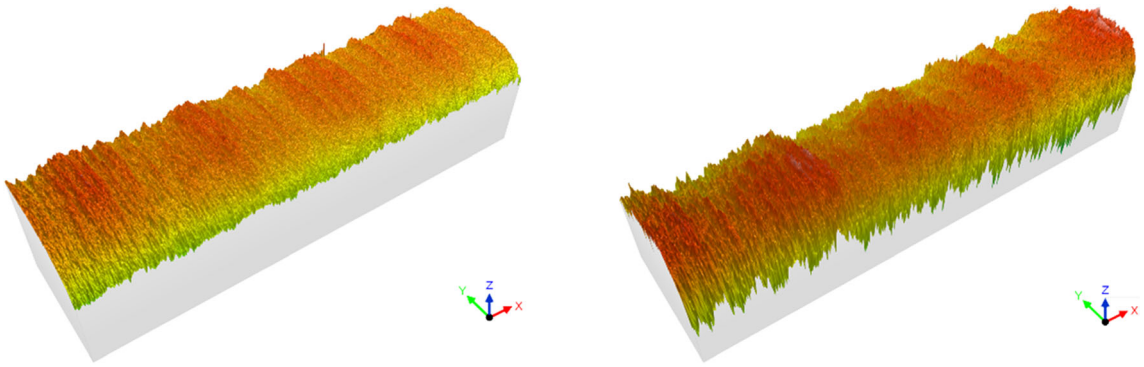

Fig. 7 3D views of the cutting front at different abrasive mass flow rates: **a** $m_a = 1239$ g/min; **b** $m_a = 354$ g/min ($u = 400$ mm/min, $p = 450$ MPa, $L = 5$ mm, $d = 8.8$ mm)

relationships cannot be directly deduced from the 3D views in these figures.

3.2 Surface roughness

In order to have a clear understanding of the specific relationships between the process parameters and the surface quality, the variable Ra was used to denote the surface roughness of the cutting front, and the influence of each parameter on the value of Ra was studied. Figure 11 a shows the surface roughness along the cutting depth at different traverse speeds. In general, the surface roughness remained relatively low throughout the cutting process and exhibited slight fluctuations in amplitude, with values of between 1 and 4, except in the region adjacent to the jet exit point. In this region, the surface roughness underwent large fluctuations, except when the traverse speed was 50 mm/min or 600 mm/min. The curves in the region of $y = 4.77$–6.39 mm are enlarged in Fig. 11b. One can see that a sharp increase in roughness began in the range of $y = 5.7$–5.9 mm, whereas a rapid decline in roughness started in the range of $y = 5.85$–6.06 mm.

The surface roughness at different abrasive mass flow rates generally exhibited the same behavior as those at different traverse speeds (Fig. 12). However, the roughness decreased slightly in the region of the initial jet entry point and thereafter continued to remain relatively constant. This may have resulted from vibration of the mechanical equipment when the jet came into contact with the workpiece in this region. In the region near the jet exit point, the roughness also increased sharply ($y = 5.8$–6.0 mm) and then rapidly decreased ($y = 6.0$–6.4 mm). It can be seen that the greater was the abrasive mass flow rate, the higher was the maximum surface roughness.

When the waterjet pressure was changed, the distribution of the surface roughness of the cutting front was as shown in Fig. 13 and was similar to that for different traverse speeds. The maximum roughness occurred at $p = 420$ MPa, and the minimum roughness occurred at $p = 320$ MPa. In addition to small fluctuations in the region of the jet entry point and sharp fluctuations in the region near the jet exit point, there were also

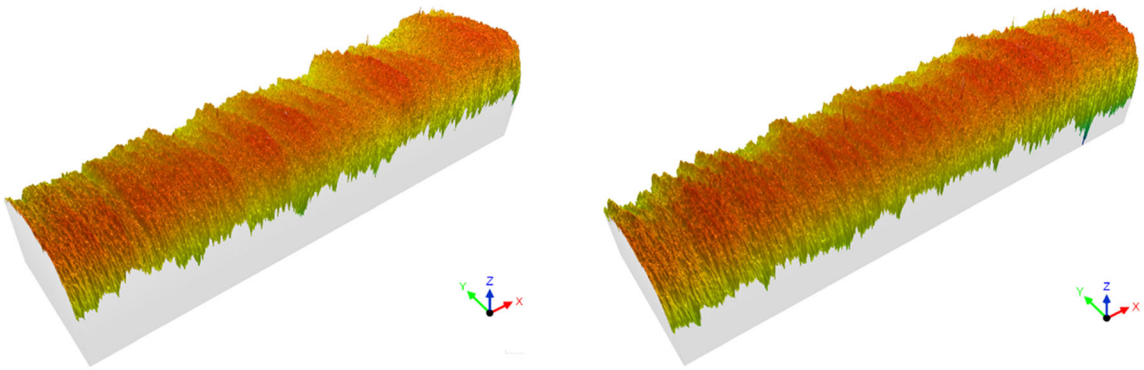

Fig. 8 3D views of the cutting front at different waterjet pressures: **a** $p = 450$ MPa; **b** $p = 300$ MPa ($u = 400$ mm/min, $m_a = 663$ g/min, $L = 5$ mm, $d = 8.8$ mm)

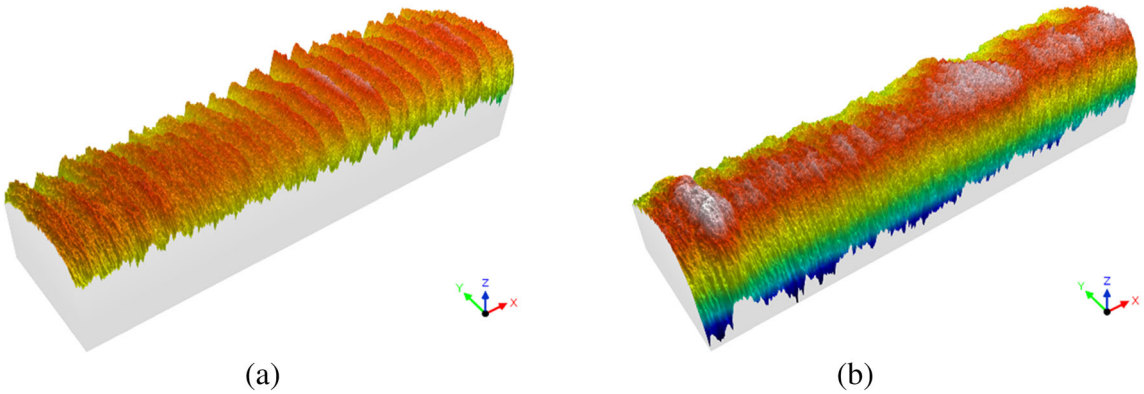

Fig. 9 3D views of the cutting front at different standoff distances: **a** $L = 5$ mm; **b** $L = 20$ mm ($u = 800$ mm/min, $m_a = 987$ g/min, $p = 450$ MPa, $d = 8.8$ mm)

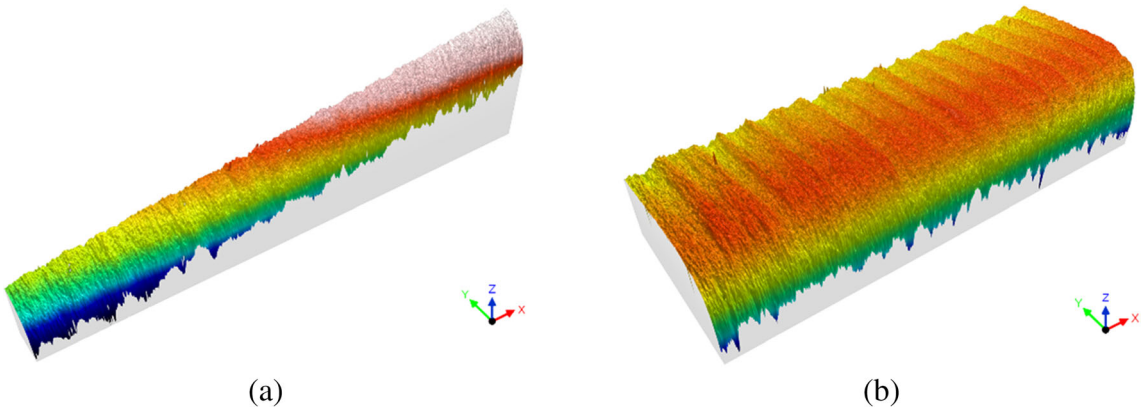

Fig. 10 3D views of the cutting front at different sample thicknesses: **a** $d = 2.2$ mm; **b** $d = 11.0$ mm ($u = 100$ mm/min, $m_a = 987$ g/min, $p = 450$ MPa, $L = 5$ mm)

small fluctuations in the intervening area. These fluctuations may be attributed to the instability of the booster device and vibrations of the cutting platform.

When the standoff distance was used as the variable, the curve of the roughness as a function of the cutting depth exhibited similar results to those for the other cutting parameters.

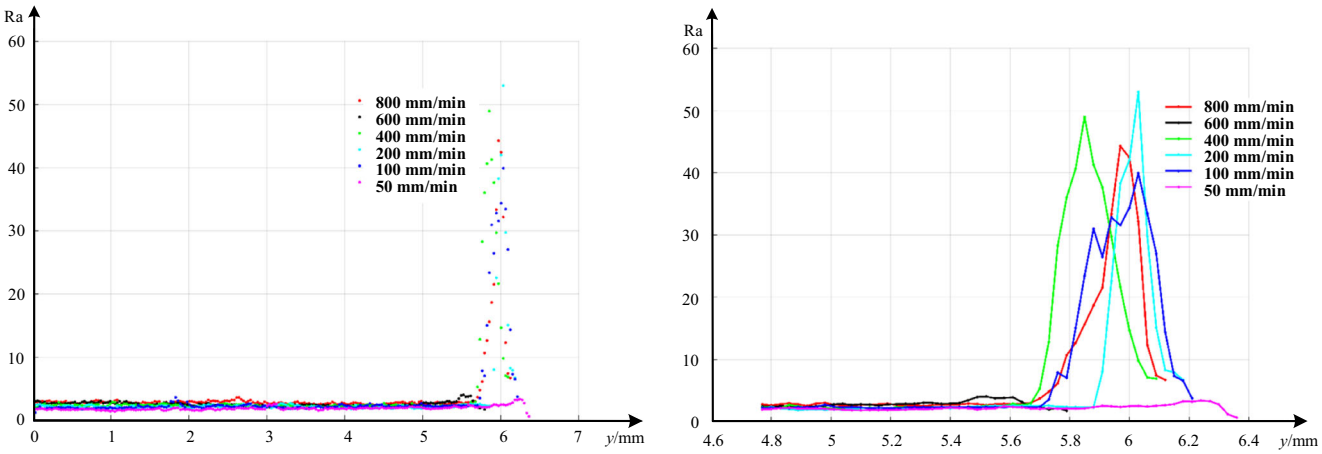

Fig. 11 Effect of traverse speed on surface roughness: **a** surface roughness along the cutting depth; **b** surface roughness in the range of $y = 4.77$–6.39 mm ($m_a = 987$ g/min, $p = 450$ MPa, $L = 5$ mm, $d = 6.8$ mm)

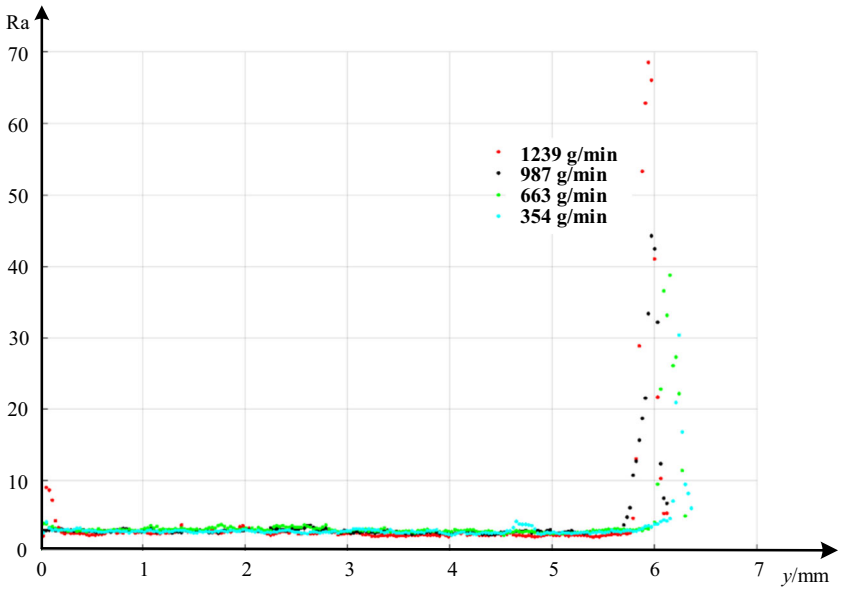

Fig. 12 Effect of abrasive mass flow rate on surface roughness ($u = 800$ mm/min, $p = 450$ MPa, $L = 5$ mm, $d = 6.8$ mm)

According to an enlarged view of the region near the jet exit point (Fig. 14b), the curve for $L = 15$ mm started to increase and then decline first in this region, and the peak value of the fluctuations was also the largest among those for all the operational conditions.

The effects on the surface roughness of the sample thickness are presented in Fig. 15; there were large fluctuations in amplitude in the region near the jet exit point. Among the samples, the workpiece with a thickness of 4.5 mm had the largest range of fluctuations, whereas the workpiece with a thickness of 8.8 mm had the smallest range.

3.3 Three-zone cutting front model

From Figs. 11, 12, 13, 14, and 15, one can see that the roughness remained relatively stable in most areas of the cutting front and displayed large fluctuations only in some confined regions, mainly those near the jet entry and jet exit points. In the region of the jet entry point, the roughness either increased from zero to the average amplitude or increased first and then decreased to a stable value of Ra in the range of 0–10 for $y =$ 0–0.2 mm. In the middle cutting zone, the roughness remained relatively stable with small fluctuations, and the value of Ra

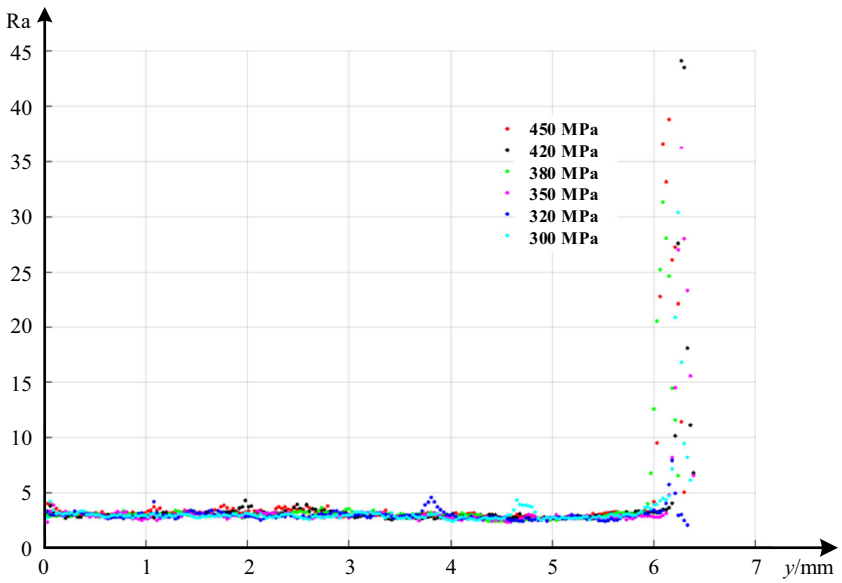

Fig. 13 Effect of waterjet pressure on surface roughness ($u = 800$ mm/min, $m_a = 663$ g/min, $L = 5$ mm, $d = 6.8$ mm)

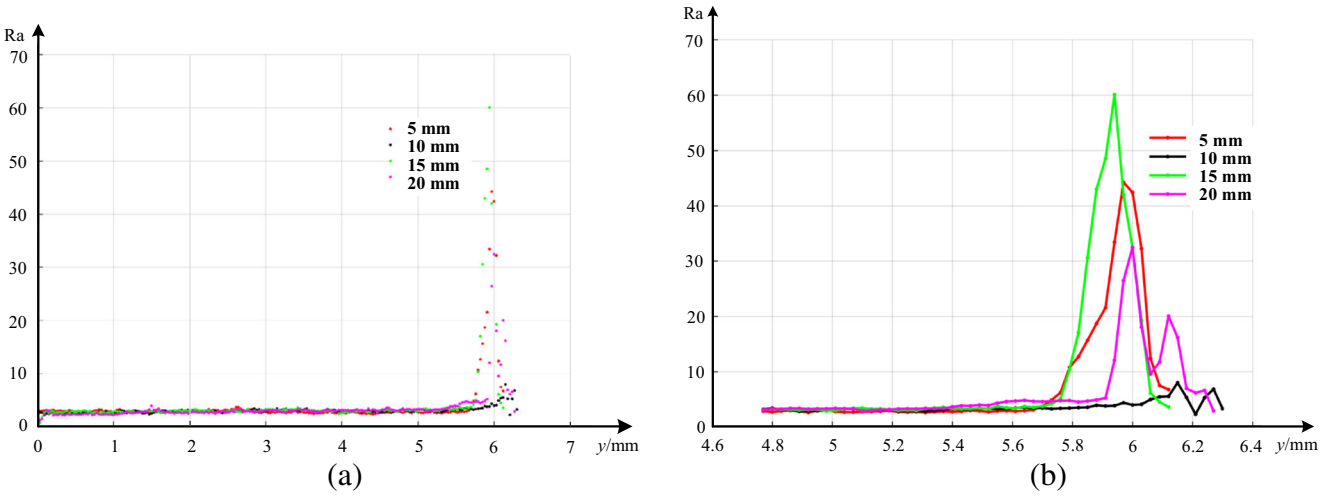

Fig. 14 Effect of standoff distance on surface roughness: **a** surface roughness along the cutting depth; **b** surface roughness in the range of $y = 4.77–6.39$ mm ($u = 800$ mm/min, $m_a = 987$ g/min, $p = 450$ MPa, $d = 6.8$ mm)

was basically in the range of 2–5. In the region near the jet exit point, the roughness exhibited large fluctuations, and the maximum value of Ra reached about 62. This is basically in agreement with Arola and Ramulu's [20] experimental results. The distribution of the surface roughness of machined CFRP indicated the presence of three distinct regions along the cutting depth, each of which exhibited unique surface features. According to the experiment conducted by Arola and Ramulu [20], these three regions are the initial damage region at the jet entry, the smooth cutting region in the intervening area, and the rough cutting region near the jet exit point. In order to devise a better division of the cutting front according to the ranges of the fluctuations in roughness, the dimensionless cutting depth, which is normalized by the corresponding sample thickness, was introduced. Using the dimensionless cutting depth as the abscissa, the roughness distribution for different sample thicknesses displayed the same behavior, as illustrated in Fig. 16, and the cutting front was divided into three distinct regions according to the degree of roughness. These three regions are categorized as follows.

Initial damage region (IDR): The initial damage region is located at the jet entry point. According to the three-zone cutting front model proposed by Arola and Ramulu for a graphite/epoxy laminate [20], the initial damage region at the jet entry point has a direct relationship with the diameter of the AWJ nozzle. According to our experimental data, the

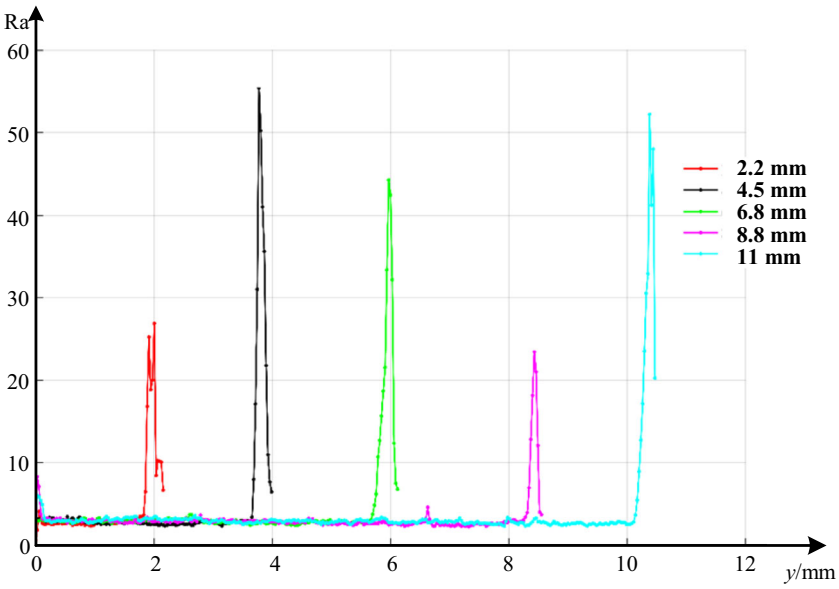

Fig. 15 Effect of sample thickness on surface roughness ($u = 800$ mm/min, $m_a = 987$ g/min, $p = 450$ MPa, $L = 5$ mm)

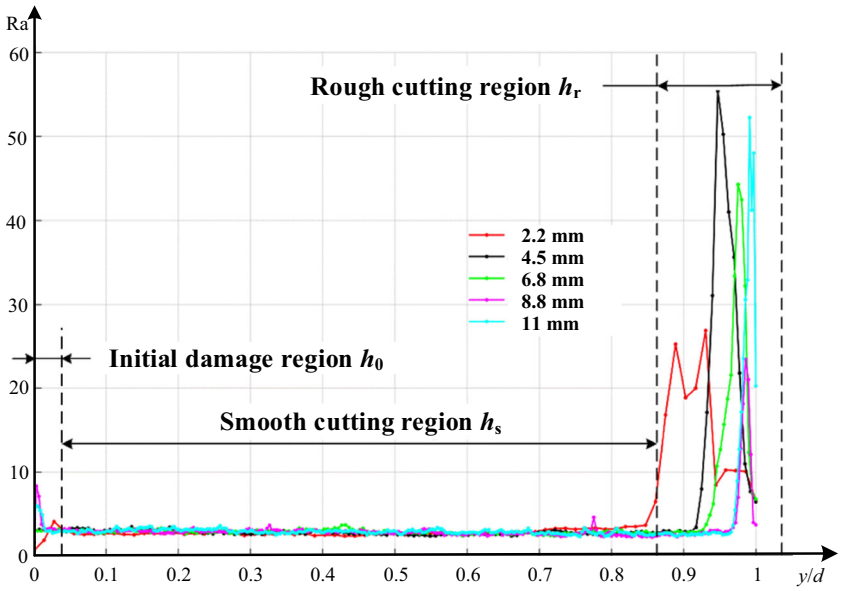

Fig. 16 Three-zone cutting front model of CFRP workpiece subjected to AWJ cutting (u = 800 mm/min, m_a = 987 g/min, p = 450 MPa, L = 5 mm)

length of this region in CFRP was about 0.2D (where D is the diameter of the AWJ nozzle, which was 1 mm in this experiment).

Smooth cutting region (SCR): The surface is smooth and the Ra value is about 2–5 in this region because the AWJ acts on this region directly and the jet energy is sufficient for stable cutting. The results of the above experiments revealed that the end of the SCR is located in the range of y/d = 0.83–0.92. The analysis of the influence of the cutting parameters on the surface roughness along the penetration direction indicated that the range of the SCR has a direct relationship with the process parameters.

Rough cutting region (RCR): The surface of this region has more obvious stripes and grooves, with the result that the boundary between the SCR and the RCR of the cutting front can be observed clearly. This roughness may be caused by two reasons, of which one is the fact that the energy of the AWJ is severely depleted when it reaches this area, so that the material cannot be destroyed and removed effectively. The other reason is frictional collisions between particles and particles, particles and water, and particles and surfaces because of the reflection of the abrasive water jet.

3.4 Influence of process parameters on the length of the SCR

In the cutting process, the SCR, where Ra is relatively low and stable, has an important influence on the surface quality. The point at which Ra = 5 is defined as the boundary between the smooth and rough cutting regions from the experimental data, from which the length of the SCR was determined. The variable h_s is used to denote the length of the SCR in the jet penetration direction.

Figure 17 illustrates the influence of the process parameters on the length of the SCR. It appears from Fig. 17a that the cutting depth of the SCR reached a maximum at a traverse speed of 200 mm/min. As for the abrasive mass flow rate, the length of the SCR reached a minimum at an abrasive mass flow rate of approximately 1000 g/min but exhibited no maximum value, as illustrated in Fig. 17b. In order to ensure high quality of the cutting front, it is necessary to avoid abrasive mass flow rates in the intermediate range in the figure. However, the cutting performance and efficiency of the penetrating jet will be reduced at a low abrasive mass flow rate, and the piping system will be blocked as a result of a high abrasive mass flow rate. Therefore, the selection of the abrasive mass flow rate needs to be considered comprehensively. As shown in Fig. 17c, the relationship of the SCR length with the waterjet pressure exhibited large fluctuations in amplitude. In order to improve the process efficiency and the quality of the machined surface of CFRP, it is suggested that the pressure should preferably be in the range of 300–345 MPa. Figure 17 d shows that a standoff distance in the range of 7–13 mm resulted in a greater SCR length. This may have occurred because the jet expanded over too broad an area when the standoff distance was too great, whereas too short a standoff distance may have caused mechanical vibration and possible scratching between the nozzle and the workpiece. Figure 17 e presents the relationship between the relative length of the SCR and the sample thickness. It is recommended that the sample

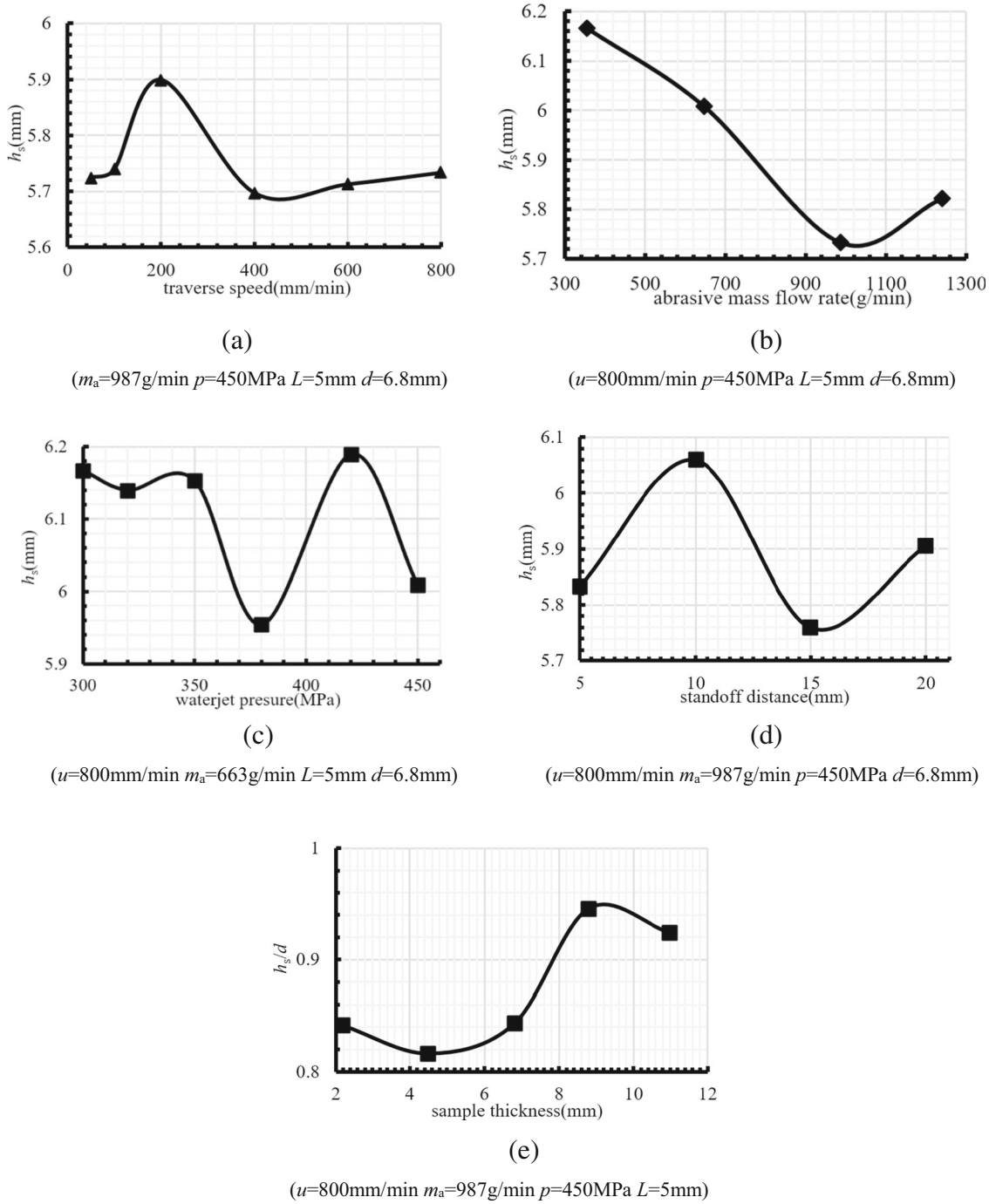

Fig. 17 Influence of process parameters on the length of the smooth cutting region, the parameters are **a** traverse speed, **b** abrasive mass flow rate, **c** waterjet pressure, **d** standoff distance, and **e** sample thickness, respectively

thickness should be in the range of 8–10 mm in order to obtain the greatest relative length of the SCR.

4 Conclusions

An experimental study was conducted to reveal the influence of the process parameters on the surface morphology of the cutting front in AWJ machining of CFRP. The results of this study were analyzed, and the following conclusions were reached:

1. Waviness patterns or stripes and grooves can be seen in the three-dimensional height distribution of the landscape profile of the cutting front, and the cyclical kerf profile in the feed direction indicated that the AWJ cutting process

was cyclical. The kerf profile was influenced by the traverse speed, abrasive mass flow rate, waterjet pressure, standoff distance, and sample thickness. Among these factors, traverse speed was found to have a remarkable effect on the kerf profile, and a moderate traverse speed was more conducive to achieve high overall surface quality.

2. The three-zone cutting front model was proposed according to the surface roughness along the penetration direction, and the cutting front was divided into three distinct regions. These three regions were the initial damage region at the jet entry point with the length of 0.2D, the smooth cutting region in the intervening area with the end in the range of $y/d = 0.83–0.92$, and the rough cutting region near the jet exit point.
3. Extension of the SCR may be accomplished with suitable process parameters. It is suggested that the length of the smooth cutting zone reached a maximum at a traverse speed of 200 mm/min, a waterjet pressure of 300–345 MPa, a standoff distance of 7–13 mm, and a sample thickness of 8–10 mm. There is no maximum value in the curve of the cutting depth in the SCR versus the abrasive mass flow rate, which needs to be chosen according to the actual situation.

Acknowledgments The work described in this paper was supported by the National High Technology Research and Development Program (National 863 Project) with the number of 2015AA043401.

References

1. Zhu CL (2012) Applications of carbon fiber composites. Adv Mater Res 378-379:121–124. https://doi.org/10.4028/www.scientific.net/AMR.378-379.121
2. Wu MY, Tong ML, Wang YW, Ji W, Wang Y (2013) Study on carbon fiber composite materials cutting tools. Applied Mechanics & Materials 401-403:721–727. https://doi.org/10.4028/www.scientific.net/AMM.401-403.721
3. Wang J (1999) A machinability study of polymer matrix composites using abrasive waterjet cutting technology. J Mater Process Tech 94(1):30–35. https://doi.org/10.1016/S0924-0136(98)00443-9
4. Riveiro A, Quintero F, Lusquiños F, Val JD, Comesaña R, Boutinguiza M, Pou J (2012) Experimental study on the CO2 laser cutting of carbon fiber reinforced plastic composite. Composites Part A 43(8):1400–1409. https://doi.org/10.1016/j.compositesa.2012.02.012
5. Mazurkiewicz M (2000) A manufacturing tool for a new century. J Mater Process Technol 106(1):112–118. https://doi.org/10.1016/S0924-0136(00)00600-2
6. Momber AW, Kovacevic R (1998) Principles of abrasive water jet machining. Springer London. https://doi.org/10.1007/978-1-4471-1572-4
7. Paul S, Hoogstrate AM, Luttervelt CAV, Kals HJJ (1998) An experimental investigation of rectangular pocket milling with abrasive water jet. J Mater Process Tech 73(1–3):179–188. https://doi.org/10.1016/s0924-0136(97)00227-6
8. Çaydaş U, Hasçalık A (2008) A study on surface roughness in abrasive waterjet machining process using artificial neural networks and regression analysis method. J Mater Process Tech 202(1):574–582. https://doi.org/10.1016/j.jmatprotec.2007.10.024
9. Thongkaew K, Wang J, Yeoh GH (2016) An investigation of hole machining process on a carbon-fiber reinforced plastic sheet by abrasive waterjet. Adv Mater Res 1136:113–118. https://doi.org/10.4028/www.scientific.net/amr.1136.113
10. Li W, Zhu H, Wang J, Huang C (2016) Radial-mode abrasive waterjet turning of short carbon–fiber-reinforced plastics. Mach Sci Technol 20(2):231–248. https://doi.org/10.1080/10910344.2016.1165836
11. Alberdi A, Suárez A, Artaza T, Escobar-Palafox GA, Ridgway K (2013) Composite cutting with abrasive water jet. Procedia Eng 63(63):421–429. https://doi.org/10.1016/j.proeng.2013.08.217
12. Liu D, Huang CZ, Wang J, Zhu HT, Yao P, Liu ZW (2013) Study on the effect of standoff distance on processing performance of alumina ceramics in two modes of abrasive waterjet turning patterns. Adv Mater Res 797:21–26. https://doi.org/10.4028/www.scientific.net/AMR.797.21
13. Zeng J, Kim TJ (1996) An erosion model of polycrystalline ceramics in abrasive waterjet cutting. Wear 193(2):207–217. https://doi.org/10.1016/0043-1648(95)06721-3
14. Shukla R, Singh D (2017) Experimentation investigation of abrasive water jet machining parameters using Taguchi and evolutionary optimization techniques. Swarm Evol Comput 32:167–183. https://doi.org/10.1016/j.swevo.2016.07.002
15. Patel D, Tandon P (2017) Experimental investigations of gelatin-enabled abrasive water slurry jet machining. Int J Adv Manuf Technol 89(1–4):1–16. https://doi.org/10.1007/s00170-016-9154-7
16. Hashish M (1984) A modeling study of metal cutting with abrasive waterjets. J Eng Mater Technol Asme 106(1):88. https://doi.org/10.1115/1.3225682
17. Chen L, Siores E, Wong W (1996) Kerf characteristics in abrasive waterjet cutting of ceramic materials. Int J Mach Tool Manu 36(11):1201–1206. https://doi.org/10.1016/0890-6955(95)00108-5
18. El-Domiaty AA, Abdel-Rahman AA (1997) Fracture mechanics-based model of abrasive waterjet cutting for brittle materials. Int J Adv Manuf Technol 13(3):172–181. https://doi.org/10.1007/bf01305869
19. Zeng J, Kim TJ (1992) Development of an abrasive waterjet kerf cutting model for brittle materials. Springer Netherlands https://doi.org/10.1007/978-94-011-2678-6_33
20. Arola D, Ramulu M (1996) A study of kerf characteristics in abrasive waterjet machining of graphite/epoxy composite. J Eng Mater Technol 118(2):256–265. https://doi.org/10.1115/1.2804897
21. Ramulu M, Arola D (1994) The influence of abrasive waterjet cutting conditions on the surface quality of graphite/epoxy laminates. Int J Mach Tool Manu 34(3):295–313. https://doi.org/10.1016/0890-6955(94)90001-9
22. Yanaida K (1982) The breakup of a high-speed liquid jet in air. 大阪府立工業高等専門学校研究紀要. https://doi.org/10.24729/00008020
23. Hashish M (1989) A model for abrasive-waterjet (AWJ) machining. J Eng Mater-T 111(2):154–162. https://doi.org/10.1115/1.3226448
24. Ozcelik B, Oktem H, Kurtaran H (2005) Optimum surface roughness in end milling Inconel 718 by coupling neural network model and genetic algorithm. Int J Adv Manuf Technol 27(3–4):234–241. https://doi.org/10.1007/s00170-004-2175-7
25. Piegl L, Tiller W (1997) The NURBS book. https://doi.org/10.1016/0010-4485(96)86819-9